Reconstruction of Aircraft Trajectories from AMDAR Weather Reports

CLEMENS DRÜE

Umweltmeteorologie, Universität Trier, Trier, Germany

(Manuscript received 21 May 2010, in final form 14 December 2010)

ABSTRACT

It is well known that aircraft-based meteorological measurements exhibit systematic errors depending on various flight dynamic parameters. It is also widely assumed that operational Aircraft Meteorological Data Relay (AMDAR) weather reports by commercial aircraft are affected in a similar way. However, so far, it is not possible to study such systematic errors, because datasets that contain both AMDAR reports and flight dynamic variables are not available. To overcome this deficiency, a method was developed to reconstruct the flight trajectories of aircraft using just the aircraft type and operational AMDAR reports. Because AMDAR reports do not contain information on the flight plan, origin, destination, or the motion vector of the airplane, it is not possible to employ a trajectory solver as used by air traffic control. Instead, the method uses groups of trajectory templates that are fitted to AMDAR data taken during approach or departure. This algorithm allows estimation of the heading, true airspeed, aircraft mass, roll state, pitch angle, and angle of attack of the reporting aircraft for each AMDAR report. For verification, the algorithm was applied to navigation data gathered from two Airbus-manufactured aircraft, of which one is in commercial service and one is used for aviation research. From a total of 48 profiles, a very good agreement of reconstructed and measured values was found.

1. Introduction

The Aircraft Meteorological Data Relay (AMDAR) program of the World Meteorological Organization (WMO) was initiated to employ existing meteorological equipment and data links [Aircraft Communications Addressing and Reporting System (ACARS)] on commercial jet aircraft to acquire upper-air measurements in real time (WMO AMDAR Panel 2007). AMDAR data contain at least time, position, altitude, temperature, and wind speed and direction. A few aircraft additionally carry prototype humidity sensors (Helms et al. 2009), but mixing ratio is rarely reported.

AMDAR data are extensively used as input to numerical weather prediction models (Moninger et al. 2003). Operational quality control is essentially ensured by monitoring the differences between AMDAR reports and the model background (see Drüe et al. 2008, for more details). The differences are typically so small (Cardinali et al. 2003) that forecast centers put AMDAR data into the highest of all confidence classes (Schraff and Hess 2002).

The robustness of the operational measurement systems used is without doubt, due to the strict regulations applied (e.g., see FAA 1968, 1995). Nevertheless, the allowed tolerances are defined by flight engineering needs, not by the requirements for meteorological applications.

In addition to instrument uncertainties, it is known that airborne measurements can have significant errors caused, for example, by variations in speed or load or uneven orientation during maneuvers (e.g., see Drüe and Heinemann 2001; Cooper and Baumgartner 1989; Painting 2003). Such systematic errors are mostly well correlated with flight dynamic parameters (see, e.g., Vörsmann 1990; Nacass 1992). By comparing AMDAR reports to other measurements or numerical forecast models, it was found that the resulting errors of AMDAR reports usually consist of a smaller random and a larger systematic contribution (Drüe et al. 2008, 2010; Ballish and Kumar 2008). The systematic contribution was shown to be associated with aircraft type and height (Drüe et al. 2008; Ballish and Kumar 2006) as well as with season (Ballish and Kumar 2008; Drüe et al. 2010).

During these previous investigations, indications of further systematic dependencies of AMDAR data errors on the flight dynamic state also have been found. From flight testing experience (Stoliker et al. 2005), the following flight dynamic parameters have been identified as

Corresponding author address: Clemens Drüe, Umweltmeteorologie-FB VI, Universität Trier, 54286 Trier, Germany.
E-mail: druee@uni-trier.de

DOI: 10.1175/2011JTECHA1499.1

candidates for being most influential (A. Hoff 2007, personal communication): heading, sideslip, pitch and roll angles, airspeed (or Mach number), and load (''weight over delta''; e.g., see Stoliker et al. 2005). AMDAR reports, however, do not contain such information, except for a flag indicating that the roll angle exceeds a threshold of 5° (Painting 2003). However, not all participating airlines set this flag accordingly.

The objective of the current investigation, hence, is to develop a method to retrieve the actual trajectory and as many flight dynamic parameters as possible from AMDAR data. This paper is organized in the following way: After this introduction in section 1, previous efforts and available input data are described in section 2. Section 3 summarizes the algorithm and section 4 presents the verification results. The summary and conclusions are given in section 5.

2. Data and models

a. AMDAR data

1) DATA FLOW

On board a participating aircraft (a ''unit''), the AMDAR software gathers meteorological values and compiles and transmits messages via ACARS to the airline operating the unit (WMO AMDAR Panel 2007; Painting 2003). The airline converts each single report into one of the two data formats defined by the WMO: either the FM-42 (human readable) or FM-94 Binary Universal Form for the Representation (BUFR) format (Painting 2003). The converted data are transferred to the national weather service that distributes them worldwide. In this paper, we use AMDAR data from the German weather service Deutscher Wetterdienst (DWD) observation database.

To ensure the privacy of the airlines, all information on flight origin, destination, and aircraft registration is removed and most flight numbers are replaced by anonymous unit identifiers (Painting 2003). Hence, neither aircraft registration nor type or airline can be determined from AMDAR data.

The data centers of some participating weather services, however, maintain lists indicating registration, airline, and type of each unit. Although aircraft type may be available for quality control and research, aircraft registration and airline are never disseminated. Nevertheless, information on both the type and operating airline of most units was available for the present study, resulting from ongoing research cooperation with DWD. Because the publication of this information is not permitted, no unit numbers will be specified in the following and specific airlines will referenced by randomly chosen single letters ''A''–''K.''

2) AMDAR SOFTWARE

Although some airlines have their own software, there are two standards established (Stickland 2002): The first is ACARS Teledyne Aircraft Conditioning and Management System (ACMS) AMDAR software (AAA), which was developed from the original WMO specifications and is freely available. The second is ARINC-620 Meteorological Report, which is the industry standard issued by Aeronautical Radio Incorporated (ARINC).

Both standards minimize the number of digits transmitted via ACARS to save telecommunication costs and ensure timely transmission. One result is that both standards strip seconds from both time and the latitude–longitude position of the report (Painting 2003). After this, AMDAR data never contain seconds, although the format of distributed data has room for them (Painting 2003).

Another result is that if a high initial data rate is chosen after takeoff, then no actual position information is transmitted by ARINC-620 software, in order to squeeze more reports in one transmission block. The position distributed with such reports is generated on the ground by linear interpolation. Or, in case of at least one airline, the position of the first data point is simply repeated. We will refer to such ground-generated position values as ''faked positions'' hereafter. Faked positions can be marked by setting a flag in the FM-94 format, but apparently not every airline sets the flag accordingly. In the case of increased roll angle a flag in FM-94 format can be set, and in the case of increased roll or pitch angle ''unsteady flight'' can be reported as flight phase, instead of ''ascent'' or ''descent'' (Painting 2003) but again, apparently not every airline uses such flagging.

As a consequence of such limited time and position resolution and unreliable quality flags, it is almost impossible to know the actual trajectory, or any flight dynamic parameters, from AMDAR data alone.

3) COLLECTION STRATEGY

AMDAR data are collected following various schemes, at fixed time intervals, at fixed geographic positions, or at fixed pressure levels during ascent and descent (AMDAR Panel 2010, personal communication). The European Regional AMDAR Program (E-AMDAR) mostly collects data at a high rate during selected ascents or descents, yielding vertical atmospheric profiles (Pastre 2000), while the U.S. national program and others collect data continuously throughout all flight phases.

The need to develop an error model for level flight, however, seems less urgent because en route flight is usually straight, even, at cruise speed, and in clean configuration [with flaps fully retracted; see Stengel (2004)]. Conditions are nominal with respect to sensor

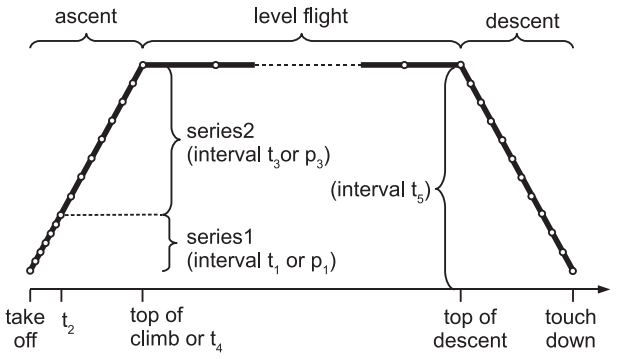

FIG. 1. Definition of flight phases, timer values t_1–t_5, and pressure intervals p_1 and p_3 used in the text.

calibrations for this phase of flight and the expected errors are minimal (Stickney et al. 1994). Our study hence focuses on ascent and descent.

In ascent and descent, the WMO specification allows for observations at fixed time intervals or at fixed pressure levels (Painting 2003). Observations should be denser near the ground to better resolve the atmospheric boundary layer (see Fig. 1). To determine the data collection schemes in use, the number of data in the first 12 min was counted for every profile taken over Europe in January 2008. The results were compared to the number of data per minute calculated for all possible combinations of $t_{1\ldots5}$ and $p_{1,3}$. It was found that most aircraft of the same airline share an identical scheme and timer values. Most of the schemes detected to be typical for a fleet were confirmed by AMDAR Panel members (2007, 2009 personal communication). However, a fraction of most fleets do not use the typical scheme, probably because of incoherent software or leased aircraft.

b. BADA model

Base of Aircraft Data (BADA) is an aircraft performance model (APM) developed by the EUROCONTROL Experimental Center (EEC) mainly for trajectory simulation and prediction by air traffic management (ATM) facilities. It contains performance characteristics and operating procedure data for a total of 294 supported (or equivalent) types EEC (2009b).

BADA uses a total energy model (TEM), which assumes that all of the energy supplied by the engines that exceeds the energy loss resulting from drag is transformed into potential energy (EEC 2009b):

$$(T - D) - m_{\mathrm{ac}}\, g_n \frac{w}{v_{\mathrm{as}}} = 0, \qquad (1)$$

with T the engine thrust, D the aircraft drag, m the aircraft mass, g_n the gravitational acceleration, w the vertical speed, and v_{as} the airspeed.

The BADA model for each aircraft is based on an operations performance model and airline procedure model (EEC 2009a). The operations performance model defines aircraft drag, thrust, and fuel consumption depending on altitude, mass, speed, and aerodynamic configuration (i.e., flap setting). The airline procedure model defines the typical aircraft operation characteristics, which include takeoff and landing speeds, standard cruising speed, and the acceleration or deceleration profile during ascent or descent, respectively, which includes the usual choice of the aerodynamic configuration. The empirical coefficients of each BADA model are determined by the coupled multivariate nonlinear fitting of model trajectories to measured aircraft positions (see EEC 2009a, for details).

The model allows a number of input parameters to be set, but when they were varied in reasonable ranges it turned out that for the purposes of this study it is sufficient to use the precalculated performance table data (PTD) provided within BADA.

In the BADA documentation, there is no clear distinction between altitude, that is, vertical distance to the sea level, and height, that is, vertical distance to the surface. Because the present study mainly focuses on (the lower part of) ascent and descent, the BADA vertical coordinate is associated to height in the following.

c. Trajectory models

Recorded data from AMDAR units cannot be obtained because the flight data recorder (FDR) stores only a limited time history and can only be read out after dismantling it from the aircraft (Lufthansa Technik 2009, personal communication).

In Drüe et al. (2008), for each of three consecutive data points a circle was fitted and the direction of the tangent at the center point was used as heading. However, results are not acceptable if the spacing of the actual positions where AMDAR data are taken is on the order of or below the resolution of position.

Air traffic control (ATC) radar tracks aircraft with a time resolution of several seconds, including the height transmitted by the aircraft transponder (Duke 2009). However, AMDAR reports cannot be associated with radar tracks because of the missing aircraft registration and flight number.

ATC uses trajectory prediction or a so-called trajectory solver for planning the flow of aircraft through control sectors and to schedule arrival times (Erzberger and Tobias 1986; Slattery and Zhao 1997). Although such models are optimized for prediction of the vertical trajectory (i.e., height versus time), they are potentially usable for purposes of the present study. Using such models is, however, prevented by the fact that they are factually not

available to researchers outside the organizations that develop them.

3. Algorithm description

a. Data preparation

For each profile, the AMDAR data are retrieved from a database and sorted by increasing time and decreasing (in ascent) or increasing (in descent) static pressure, the aircraft type is read from the list of units and the corresponding performance coefficients are extracted from BADA.

To facilitate geometric calculations, AMDAR positions are projected onto an x–y plane by an oblique stereographic projection using the Conformal Map Function (CMAPF) version 2.0 routines (Taylor 1997). For each profile, the position of the lowest data point is chosen as the projection center.

During approach, aircraft often have to interrupt their descent at certain altitudes. If they undershoot such an altitude, then a slight climb might be required. If in such cases, multiple AMDAR reports are generated within the same minute, then sorting them by ascending static pressure does not yield the correct order of the data points. Hence, for each possible permutation, the algorithm calculates the distance needed to travel from the last position in the preceding minute $j - 1$ along all of the data points in minute j to the first position in the following minute $j + 1$, and the permutation with the shortest distance traveled is chosen.

b. Scheme recognition

Detection of a known collection scheme not only easily yields report seconds (a more general method will be described in section 3), but also provides information about positions being faked. Therefore, a method was developed that tests if one of the known schemes applies. It evaluates the first 6 min of an ascent or the last 6 min of a descent, respectively, and calculates the ARINC timer values, if needed.

The success of this procedure was tested by calculating the probability of detection (POD), which gives the percentage of cases in which the detected scheme matches the scheme that is typical for the airline operating that particular unit. Table 1 summarizes results for the AMDAR profiles taken in January 2008 over Europe. Except for airlines F, H, and K (which have reported only a small number of profiles), the POD is always well above 50%. The average POD is even 80% in ascent and almost 95% in descent.

For example, in case of airline B about 7% of the fleet are aircraft with different avionics (Giraud 2010) that typically implement pressure-based reporting (AMDAR Panel 2009, personal communication). Hence, POD cannot reach values of more than roughly 93%. With respect to such general conditions, the calculated POD values seem rather satisfying.

TABLE 1. Probability of detection of the data collection schemes for (top) ascent and (bottom) descent. Collection schemes: "?" unknown, "1pt" one-phased timed, "2pt" two-phased timed, "pl" pressure levels, or "A" two-phased timed starting at full minute. Data represent the E-AMDAR profiles taken over Europe in January 2008.

Airline	No.	Collection scheme					POD (%)
		?	1pt	2pt	pl	A	
Ascent (average POD = 80.4%)							
A	257					X	91
B	103		X				76
C	50				X		64
D	45			X			78
E	33			X			76
F	11			X			36
G	7			X			57
H	6			X			0
I	3				X		100
Descent (average POD = 94.2%)							
A	248		X				97
B	102		X				100
D	60		X				100
C	50	X			X		100
E	32		X				94
F	11		X				0
K	7		X				29
H	6		X				33
I	3	X			X		100

c. Trajectory fitting

1) First guess

In case a particular reporting scheme is detected, all faked data point positions are flagged. In the case of an unknown two-phased timed or pressure-triggered ascent scheme, data taken at a higher rate than every 15 s are assumed to be faked, except for the first data point.

From the remaining data, a first guess of the trajectory is determined. For every data point i, heading $\Phi_{pp}(i)$ is estimated from the forward difference of the data position, and the values are smoothed using a running window of a 3-min flight time. From the estimated heading, the amount $|\Delta\Phi_{pp}(i)|$ of the turn angle at each data point is calculated. In case the sense of turn is different from the last data point or the amount of the turn angle exhibits a local minimum, the value is set to zero to distinguish closely following turns. Each group of one or more consecutive data points where $|\Delta\Phi_{pp}(i)|$ exceeds a threshold value of 1.5° is regarded as a candidate for a turn. If more than five candidates are detected, then the candidates with the highest peak values are selected. If less than five candidates are detected, additional candidates are added at the center of

the longest distance between two candidates until five candidates are reached.

Based on the first guess, the aircraft trajectory is fitted. The fit is done first horizontally and then vertically, since Slattery and Zhao (1997) have demonstrated that this procedure represents a calculation cost–effective way to achieve sufficiently precise results. As in Slattery and Zhao (1997), the wind is also neglected here so that airspeed equals groundspeed for trajectory fitting.

2) HORIZONTAL

For every profile, up to six raw trajectories are composed from two templates: straight flight and a turn with a 30° bank angle (EEC 2009a). If a profile contains less than 13 (nonfaked) data points, the number of segments is limited to $N/2 - 1$, in which N is the number of data points. For each of these raw trajectories, a minimal set of parameters is optimized to minimize a cost function. The trajectory that yields the lowest cost function, that is, the best fit, is chosen as the horizontal solution.

Each raw trajectory with n_{seg} segments is constructed from the first data point and the positions of the $n_{\text{seg}} - 1$ strongest candidate turns. First and last data point are used as fly-over data points and the candidate turn positions are used as fly-by waypoints (i.e., the intersection of the straight flight segments). This choice defines the heading of each straight segment, and initially a 140-kt average speed, which is a typical value derived from the BADA model, is assumed on all straight segments. The radius of each turn is calculated from the prescribed bank angle ψ_t of 30° and the mean of the speeds on the two adjacent straight segments,

$$r_{\text{t}}(l) = \frac{1}{g_n \tan\psi_t}\left[\frac{v_{\text{seg}}(l-1) + v_{\text{seg}}(l)}{2}\right]^2, \qquad (2)$$

in which l is the number of the turn and $v_{\text{seg}}(l)$ is the average speed on segment number l. The turn center position is defined by the condition that both adjacent straight segments must be tangents to the turn circle. The positions, where the straight line segments meet the turn circles, that is, the start and end position of each turn, define the duration of each straight segment. Of all of these values, at least three per straight segment are needed to define the trajectory. In this study, heading $\Phi_s(l)$, average speed $v_s(l)$, duration $t_s(l)$ of each straight segment, and the initial position are chosen.

The cost function J_H is defined as

$$J_H^2 = \sum_{i=1}^{n_s} d_s(i)^2 + d_i^2 + d_e^2 + J_{\text{ang}}^2 + J_{\text{dist}}^2 + J_{\text{vel}}^2, \qquad (3)$$

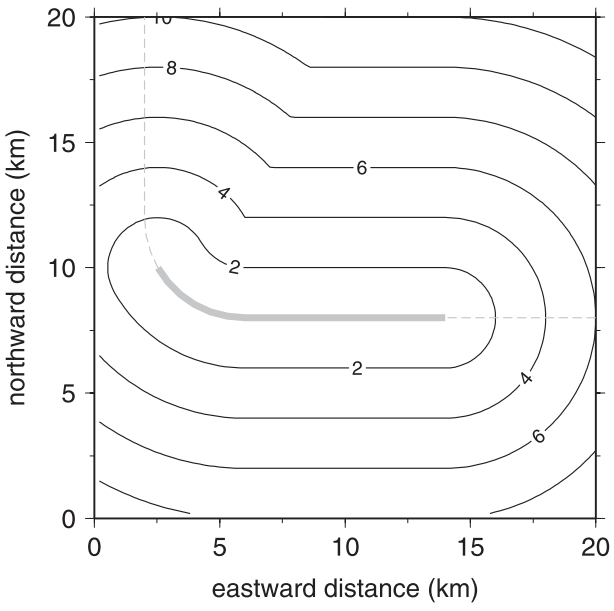

FIG. 2. Distance to a 1-min part (bold gray line) of an exemplary trajectory (dashed gray line) as function of the position. Contours give distance in kilometers.

where $d_s(i)$ is the distance of data point i to the portion of the trajectory that was passed in the minute the data point i was taken (Fig. 2). If there is no temporal overlap between the duration of the trajectory and this minute, the distance to the portion passed in the nearest minute is substituted.

Respectively, d_i and d_e are the distance between the trajectory start position and the first data point (subscript i) and the trajectory end position and the last data point (subscript e).

The quantity J_{ang} represents the sum of all turn angles. Minimizing this value prevents oscillations or loops,

$$J_{\text{ang}} = w_{\text{ang}} n_{\text{s}} \sum_{l=1}^{n_{\text{seg}}-1} |\psi_t(l)|, \qquad (4)$$

with $\psi_t(l)$ the turn angle of turn number l and the empirical weighting factor $w_{\text{ang}} = 1.5$ m per degree and data point.

The total travel distance along all straight flight segments per data point is described by J_{dist}. Minimizing this value prevents overshooting in turns without provoking a too-short trajectory,

$$J_{\text{dist}} = w_{\text{dist}} \sum_{l=1}^{n_{\text{seg}}} \frac{v_s(l) t_s(l)}{n_s}, \qquad (5)$$

with the empirical weighting factor $w_{\text{dist}} = 2.0$.

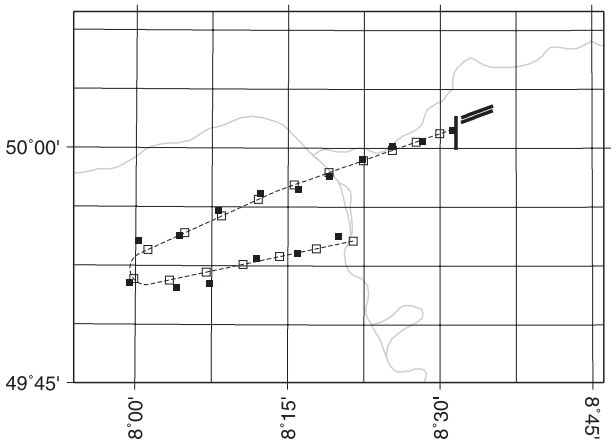

FIG. 3. Example of a fitted 2-turn trajectory. Data are taken form the descent of an Airbus A319 to Frankfurt airport (EDDF) on 5 Jul 2006. Data point positions reported by AMDAR (black squares), the fitted trajectory (dashed line), and the fitted data point positions (open squares). The three bold black lines mark the runways of Frankfurt airport.

The deviation of the average speed from the BADA model value for a flight with reference mass (EEC 2009a) is given by J_{dist}. For each straight flight segment l the data points (index i) are determined, which are taken during minutes that overlap the duration of section l. The BADA model speed is calculated for each of these data points from its height $h(i)$ and the BADA performance files for the current aircraft type EEC (2009b), and the single BADA model speeds are averaged to yield the segment mean $v_{\text{sch}}(z_{\text{avg}})$ (subscript "sch" stands for schedule),

$$J_{\text{vel}} = w_{\text{vel}}^2 \sum_{l=1}^{n_{\text{seg}}} \{[v_s(l) - v_{\text{sch}}(z_{\text{avg}})]^2 + P_{\text{oper}}\}, \quad (6)$$

with the empirical weighting factor $w_{\text{vel}} = 100$ s. The additive penalty P_{oper} is added above maximum operating speed v_{mo} and below minimum stall speed v_{st} of the aircraft type to force the speed into the operating limits of the aircraft.

Starting from the first guess, the trajectory parameters are optimized by Powell's quadratic convergent method (Press et al. 1986) until J reaches a minimum, allowing a remaining fractional tolerance of 10^{-5}.

The weight factors in Eqs. (4)–(6) were determined empirically. For each type of data collection scheme, between 2 and 12 sample profiles were selected from AMDAR data take over Europe in January and July 2008. The samples ranged in complexity from a straight departure to an approach that was interrupted in a holding pattern. The weights were varied until a trajectory was found for all of the samples that seemed reasonable by visual inspection (see Figs. 3 and 4).

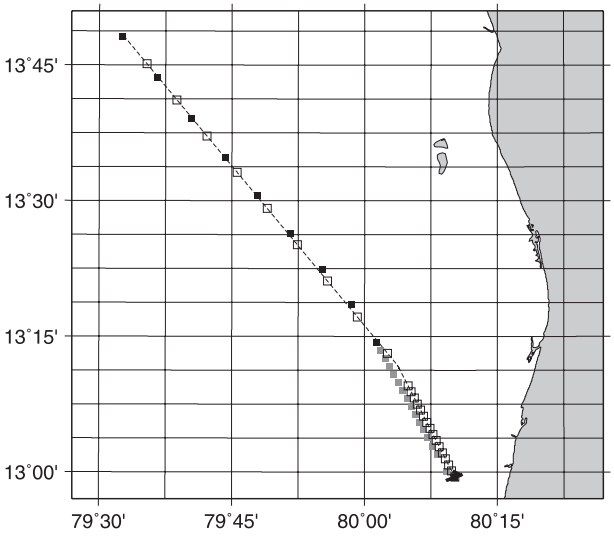

FIG. 4. Example of an ascent fitted to data from Lufthansa A340–600 "Leverkusen" departing from Chennai airport (VOMM) on 13 Aug 2008. Data are taken from the verification dataset described in section 4. Presentation as in Fig. 3, but some data points represent faked positions (gray squares).

3) VERTICAL

Because altitude is measured and reported with good accuracy, a vertical trajectory fit is only needed if the reporting scheme is pressure based or unknown. If no known scheme reproduces the observed number of data per minute, then a vertical trajectory fit is done.

(i) Known collection scheme

Applying a known scheme is strikingly difficult, because single data points may be missing, as explained in the previous section. Hence, the algorithm applies a three-pass method: First, the sequence of reporting times is modeled by assuming that the first data point is taken at the full minute. Second, the second of the first data point is varied until the modeled number of data in every minute is larger than or equal to that measured and the sum of the differences is minimal. In the third pass, the seconds of data for minutes with less data points than that modeled are estimated by interpolating time according to altitude and choosing the nearest modeled time.

(ii) Unknown collection scheme

In case of a pressure-based or unknown scheme, the algorithm also applies a three-pass method: First, for each data point with a nonfaked position, the position on the fitted horizontal trajectory that is nearest to the reported position is determined and the flight time needed to reach

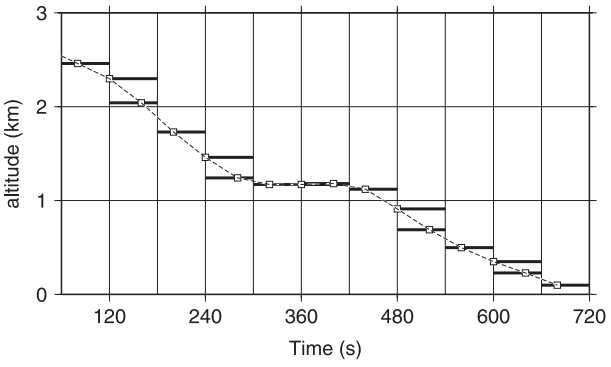

FIG. 5. Vertical profile of the descent shown in Fig. 3. The altitudes of the AMDAR reports are marked (black bars); each bar fills the one minute of the report. The fitted trajectory (dashed line) and the fitted data point positions (open squares).

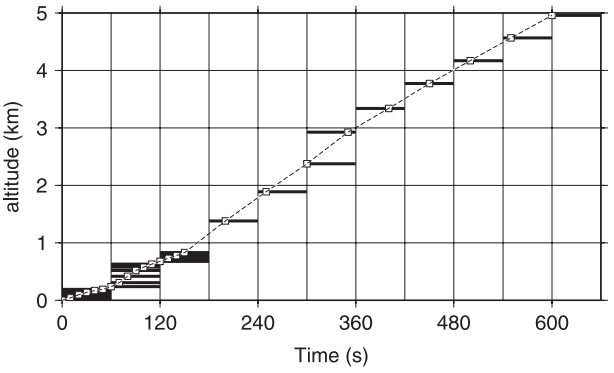

FIG. 6. Vertical profile of the ascent shown in Fig. 4. Same presentation as in Fig. 5.

this position is calculated. Second, times of data points with faked positions are linearly interpolated between the nearest data points with nonfaked positions. Third, the time of each data point is successively adjusted. It is assumed that the aircraft either performs a nominal climb (or descent, respectively) or maintains height. This assumption is applied via the cost function J_V

$$J_V = \sum_{i=1}^{n_s} \min\langle w_a(i)^2;\ \{w_a(i) - w_{\mathrm{sch}}[z(i)]\}^2\rangle, \qquad (7)$$

where $w_a(i)$ is the vertical velocity of the aircraft at data point i, calculated from the forward differences of time and altitude; $w_{\mathrm{sch}}[z(i)]$ is the BADA model average vertical speed for a nominal mass ascent or descent at altitude $z(i)$. The time of each data point is varied between the times of the neighboring data points, but not outside its original minute, until cost function J_V is minimized. This step is iterated until the seconds do not change any further.

After the seconds are estimated, the data point positions are recalculated by integrating traveled distance along the horizontal trajectory (see Figs. 5 and 6).

d. Flight dynamic state

1) SPEED

The vertical profile of the aircraft speed v_{gs} on each straight segment of the trajectory is assumed to have the same shape as the BADA reference mass ascent or descent speed profile $v_{\mathrm{sch}}(z)$, respectively; that is,

$$v_s(i) = f_s(l)\ v_{\mathrm{sch}}[z(i)], \qquad (8)$$

where $f_s(l)$ is the scaling factor for segment l.

To determine this factor, the average speed schedule for the height band between $z_i(l)$ and $z_e(l)$ corresponding to segment l is determined by integrating the time needed to climb or sink this vertical distance traveling at BADA model speed schedule $v_{\mathrm{sch}}(z)$,

$$v_{s,\mathrm{sch}}(l) = \int_{z_i(l)}^{z_e(l)} \frac{v_{\mathrm{sch}}(z)}{w_{\mathrm{sch}}(z)} dz \Bigg/ \int_{z_i(l)}^{z_e(l)} \frac{1}{w_{\mathrm{sch}}(z)}\, dz. \qquad (9)$$

Then, $f_s(l)$ is calculated as the ratio of the segment mean speed $v_s(z)$ to the mean speed schedule $v_{s,\mathrm{sch}}(l)$ from BADA. If data point i is in a turn (index l), instead of Eq. (8), then the mean scaling factor and speed of the neighboring straight segments are applied,

$$v_{\mathrm{gs}}(i) = \frac{f_s(l) + f_s(l+1)}{2}\ \frac{v_{s,\mathrm{sch}}(l) + v_{s,\mathrm{sch}}(l+1)}{2}. \qquad (10)$$

In the previous calculations, the wind was neglected, but to include the wind, it is assumed at this point that the speed values calculated from the fitted trajectory are ground speed. The track angle $\Psi(i)$, that is, the direction of the motion relative to the ground, is calculated from the geometry of the fitted trajectory. Subtracting the wind vector contained in the AMDAR data then yields the airspeed vector (see Drüe et al. 2008), that is, airspeed $v_{\mathrm{as}}(i)$ and heading $\Phi(i)$ of the aircraft at data point i are calculated.

The vertical velocity of the aircraft is calculated from the differences of altitude and time to the nearest data point that is more than 5 s away. This minimum distance was introduced to reduce numerical noise in the case of very closely spaced data.

2) AIRCRAFT MASS

Based on the BADA TEM (1), the current mass of the aircraft can be estimated because aircraft operating speeds vary with the aircraft mass (EEC 2009b),

$$v = v_{\mathrm{ref}} \sqrt{m_{\mathrm{ac}}/m_{\mathrm{ref}}}, \qquad (11)$$

where v is a current operating speed, for example, stall speed, and v_{ref} is the corresponding reference speed given for mass m_{ref}.

The BADA model equation for flight with reference mass reads

$$(T-D)_{\mathrm{ref}} - m_{\mathrm{ref}} g_n \frac{w_{\mathrm{ref}}}{v_{\mathrm{as,ref}}} = 0, \tag{12}$$

with $(T - D)$ thrust minus drag, w_{ref} the vertical speed, and $v_{\mathrm{as,ref}}$ the airspeed, all three for flight with reference mass. To estimate the mass, the simple assumption is made that the sum thrust minus drag is always equal to the BADA model reference value $(T - D) = (T - D)_{\mathrm{ref}}$. Equations (1) and (12) yield the current aircraft mass through

$$m_{\mathrm{ac}} = m_{\mathrm{ref}} \left(\frac{w_{\mathrm{ref}}}{v_{\mathrm{as,ref}}} \right) \Big/ \left(\frac{w}{v_{\mathrm{as}}} \right). \tag{13}$$

While inspecting the data, it was found that the BADA model equation has to be expanded by an additional energy sink D_+ because of additional drag, for example, that is caused by sideslip,

$$(T - D) - m g_n \frac{w}{v_{\mathrm{as,ref}}} - D_+ = 0. \tag{14}$$

Because energy can only be lost through additional drag, it is $D_+ \geq 0$. When evaluating Eq. (13) for all of the data points, it was hence expected that the computed values would be smaller or equal to the true value. Instead, it turned out that in a small number of cases the calculated mass becomes large, because D_+ becomes negative, presumably when $(T - D)$ is much different from the BADA model.

Therefore, Eq. (13) is evaluated for all data points of a profile and the lower 85% percentile value of the calculated masses is taken as estimation for m_{ac}.

3) ORIENTATION

The aircraft roll angle is set to zero on straight segments and equal to the predefined roll angle in turns.

The pitch angle is estimated from the aircraft energy balance using the residual D_+. It is assumed that D_+ is only caused by additional drag associated with a nonzero angle of attack α

$$D_+ = \alpha \frac{\partial D}{\partial \alpha}. \tag{15}$$

The drag coefficient C_D relates aircraft drag to dynamic pressure p_{dyn} and wing area S (Stengel 2004)

$$D = C_D p_{\mathrm{dyn}} S. \tag{16}$$

It can be expressed as a function of the lift coefficient C_L (EEC 2009b)

$$C_D = C_{\mathrm{D0}} + C_{\mathrm{D2}} C_L^2, \tag{17}$$

where C_{D0} and C_{D2} are empirical parameters of the BADA model associated with each aircraft type. The lift coefficient C_L is generally expressed as a linear function of the angle of attack

$$C_L = C_{\mathrm{LO}} + C_{\mathrm{L}\alpha} \alpha, \tag{18}$$

where C_{L0} is the lift coefficient at zero angle of attack and $C_{\mathrm{L}\alpha}$ gives the angle dependence (Stengel 2004). The quantity C_{L0} corresponds to the empirical parameters C_L in the BADA model. Inserting (16)–(18) in (15) yields the angle dependence of the additional drag

$$D_+ = \alpha [S p_{\mathrm{dyn}} 2\, C_{\mathrm{D2}} C_{\mathrm{L}\alpha} (C_L + C_{\mathrm{L}\alpha} \alpha)]. \tag{19}$$

As for mass estimation, it is assumed that $(T - D) = (T - D)_{\mathrm{ref}}$ and by substituting (12) for $(T - D)$ in (14) one gets

$$D_+ = m_{\mathrm{ref}} g_n \frac{w_{\mathrm{ref}}}{v_{\mathrm{as,ref}}} - m_{\mathrm{ac}} g_n \frac{w}{v_{\mathrm{as}}}. \tag{20}$$

Equating (20) and (19) then allows calculation of the angle of attack by solving

$$C_L \alpha + C_{\mathrm{L}\alpha} \alpha^2 - \underbrace{\frac{D_+}{S p_{\mathrm{dyn}} 2\, C_{\mathrm{D2}} C_{\mathrm{L}\alpha}}}_{C_q} = 0. \tag{21}$$

Unfortunately, it turned out that the resulting quadratic equation cannot be solved in about one-quarter of all cases. Closer inspection indicated that the term $C_{\mathrm{L}\alpha}\alpha$ is always one or two orders of magnitude smaller than the others. Hence, it seems reasonable to omit the term, which leads to

$$\alpha = \sqrt{|C_q / C_{\mathrm{L}\alpha}|}. \tag{22}$$

Aircraft mass, airspeed, and vertical velocity are known from the fitted trajectory. Speed schedules and aircraft-specific coefficients can be determined from BADA. Coefficient $C_{\mathrm{L}\alpha}$ is calculated by the Helmbold equation for jet aircraft with swept wings (Stengel 2004)

$$C_{\mathrm{L}\alpha} = \frac{\pi R_A}{1 + \sqrt{1 + \left(\frac{R_A}{2} \cos\Lambda \right)^2 (1 - M^2 \cos\Lambda)}}, \tag{23}$$

in which M is the Mach number, Λ is the sweep angle of the wings, and

$$R_A = l_s^2/S \tag{24}$$

is the wing aspect ratio with l_S the wing span.

Typical civil jet aircraft use a moderate sweep (Jenkinson et al. 1999) angle between 25°, for example, on Airbus A320, and 37°, on Boeing 747 (Morichon 2006). Because Λ is not included in the BADA model, the algorithm uses a fixed value of 30°. This simplification causes an uncertainty of about 7% in $C_{L\alpha}$, which corresponds to roughly only $\pm 0.1°$ in angle of attack.

Finally, pitch angle θ is calculated by adding the angle of attack to the vertical track angle θ'

$$\theta = \alpha + \theta' = \alpha + \arctan\frac{w}{v_{as}}. \tag{25}$$

4. Verification

To verify the results of the algorithm, datasets are needed that were taken by typical commercial jet aircraft and contain attitude angles as well as atmospheric variables.

The Global Aircraft Dataset (GADS; Tenenbaum 1991) collected by the State University of New York does contain such information, but unfortunately the project does not collect data during ascent and descent (J. Tenenbaum 2010, personal communication).

a. CARIBIC

The most useful dataset for this study is taken by the Civil Aircraft for the Regular Investigation of the Atmosphere Based on an Instrument Container (CARIBIC) project, which is carried out to study and monitor important chemical and physical processes in the earth's atmosphere using long-distance passenger flights (Brenninkmeijer et al. 2007).

CARIBIC regularly deploys an airfreight container with automated scientific instruments to the Lufthansa A340–600, called "Leverkusen." This aircraft is equipped with an air and particle (aerosol) inlet underneath the fuselage that is permanently installed. Along with the data of its own instrumentation, CARIBIC records navigation data from the aircraft data bus with 1-s resolution. We used the navigation data from all 22 CARIBIC flights in 2008 for validation of the algorithm. Unfortunately, AMDAR data from this aircraft were not available for all flights.

Therefore a simulator program was developed that mimics onboard software conforming to the ARINC-620 meteorological reporting standard, including data smoothing (Painting 2003). The algorithm described in section 3 was then applied to the simulated AMDAR data and the results were compared to the measured values for each data point. It should be noted that this procedure also ensures that the verification is performed with data that were not used to develop the algorithm.

TABLE 2. Regression results of estimated vs measured values for selected variables: icept denotes the regression intercept, r^2 denotes the correlation coefficient, and THdg and AOA stand for true heading and AOA, respectively.

		CARIBIC			ATRA		
Value	Unit	icept	Slope	r^2	icept	Slope	r^2
THdg	°	2.60	0.85	0.72	−0.79	1.16	0.98
Pitch	°	−0.28	0.94	0.65	1.89	1.28	0.79
Roll	°	0.03	0.23	0.08		N/a	
AOA	°	1.01	0.65	0.15		N/a	
w	m s^{-1}	0.35	0.96	0.94	−0.45	0.99	0.94
v_{as}	m s^{-1}	1.28	0.94	0.68	−0.51	0.98	0.73
v_{gs}	m s^{-1}	18.1	0.88	0.79	−0.45	1.02	0.75

Although some assumptions made in section 3 seem quite crude, the agreement is mostly very good. The average horizontal distance of the measured position to the reconstructed position is just 460 m and the mean difference between the measured and reconstructed altitude is 7.6 m. True airspeed is reconstructed with a mean difference of only 0.4 m s^{-1}. Linear regression yields a slope of 0.944 and an intercept of 1.3 m s^{-1}. The scatter, however, is greater than that of position and the regression coefficient is only 0.68 (see Table 2). The vertical speed, however, is rather well reconstructed with a slope of 0.964, an intercept of 0.3 m s^{-1}, and a regression coefficient of 0.94.

The estimated aircraft mass (Fig. 7) is 276 t on average, with 330 t after takeoff and 222 t before landing. Because the true mass values are not known, a verification of this estimate is not possible. Nevertheless the values obtained seem quite reasonable: for 32 out of 44 profiles, the estimated mass is inside the permitted weight limits, departing aircraft are heavier than arriving ones, and the average fuel burn is 90 t, which seems realistic (Jenkinson et al. 1999).

The good agreement of reconstructed and measured values promises reasonable estimation of the aircraft orientation. And indeed, true heading and pitch angle are estimated with a slope near unity, an almost zero intercept, and regression coefficients above 0.65 (see Fig. 8). The scatter of the angle of attack is rather large but still the slope is at 0.65 and the intercept is near zero. Roll angle, however, is not met very well, probably because it is prescribed as a fixed value, which is apparently less realistic than that estimated in literature (e.g., EEC 2009a; Jenkinson et al. 1999).

b. ATRA

A second, much smaller dataset was supplied by Deutsches Zentrum für Luft- und Raumfahrt (DLR)

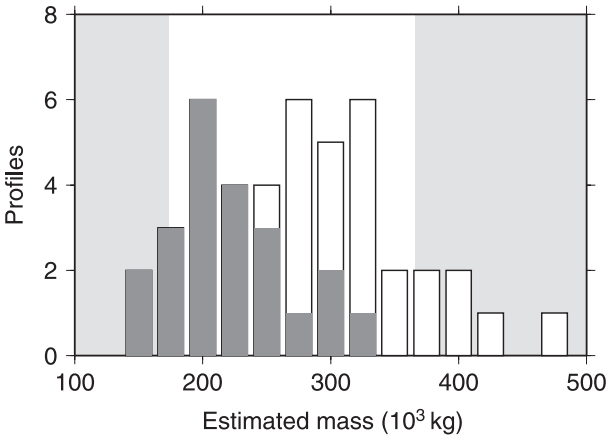

FIG. 7. Aircraft mass estimated from the validation dataset. Bars indicate the total number of profiles per 25-t bin. The gray portion of each bar gives the number of ascents. The bandwidth of permitted takeoff mass for A340–600 is marked by a white plot background.

from its Advanced Technology Research Aircraft (ATRA), which is an A320–200 modified for aviation research (Renouard-Vallet et al. 2010). Because this aircraft is rather new and mostly operates using nonstandard procedures (H. Becker, DLR, 2010, personal communication), data from only four flights could be used.

As from the CARIBIC dataset, AMDAR data were generated by the ARINC-620 simulator and used as input for the algorithm described in section 3. Because the data supplied by DLR do not contain meteorological values, wind and temperature data of the nearest operational radiosonde were used.

Compared to the CARIBIC dataset, the results are even better with respect to correlation (Table 2). The slope is even closer to unity, except for pitch. However, no measured values of the angle of attack are available and none of the generated AMDAR data points is in a turn. Hence, the ATRA dataset cannot further support the verification of roll and attack angle.

5. Summary and conclusions

To enable development of an error model for AMDAR weather reports from commercial aircraft, information about the flight dynamic state of the aircraft is needed. Because such information is neither included in the data reported nor can be substituted from other sources, a method was developed to estimate flight dynamic state variables only from AMDAR data and the aircraft type.

AMDAR data do not contain seconds, neither in position nor in time. Hence, estimating time and position of each report with greater precision is a primary goal of the algorithm. The only additional information needed is the aircraft type, which is not disclosed to the public but is available to weather data centers.

The algorithm first tries to determine the data collection scheme in order to determine (presumably) faked positions and (time) seconds of the data points. The detection was shown to exhibit a POD of 80% in ascent and 94% in descent.

The most probable horizontal trajectory is determined by consecutively fitting trajectory templates to the nonfaked AMDAR data positions. In case no known data collection scheme was detected, the seconds (time) are determined by fitting a scaled BADA vertical speed profile to the data point altitudes. From the fitted positions and times, speed, mass, and orientation are estimated applying

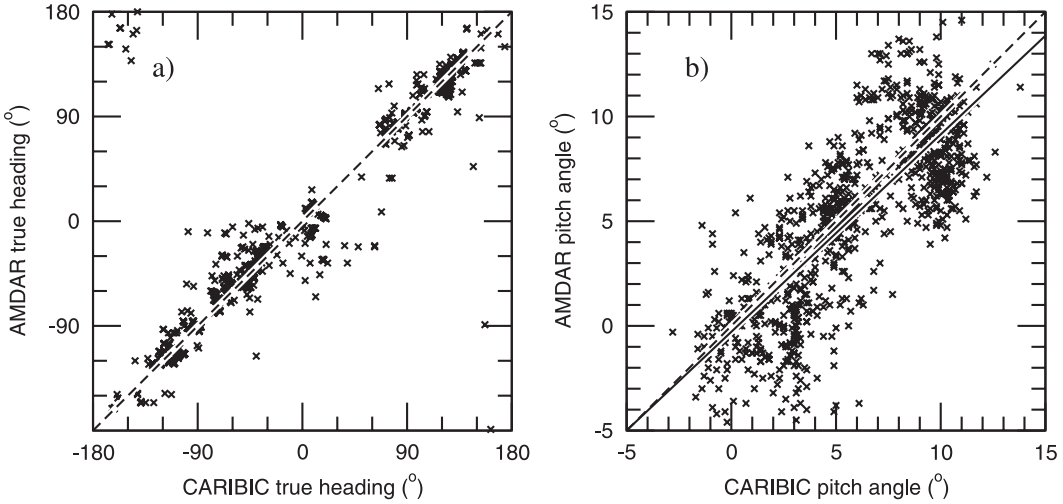

FIG. 8. Scatterplot of estimated (AMDAR) vs measured (CARIBIC) angles. (left) True heading and (right) pitch angle. The line of identity (dashed line) and the linear fit to the data (solid line).

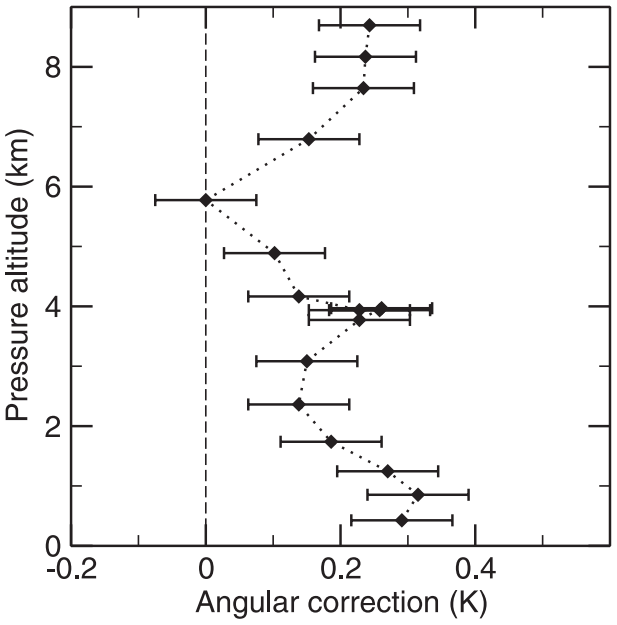

FIG. 9. Hypothetical temperature error by neglecting pitch. Data are taken from the descent shown in Fig. 3.

the BADA total energy model, assuming thrust minus drag ($T - D$) is always at its BADA reference value.

To validate the algorithm, two rare datasets of flight dynamic recordings from commercially used jet aircraft types were used. On these data, it could be shown that the new algorithm estimates the actual position with good accuracy, that is, a position with less than 0.5 km and altitude with less than 8-m average deviation. The estimated mass, although no reference data are available, appears rather reasonable and mostly keeps in the permitted mass limits. Pitch, heading, and angle of attack are estimated with rather good agreement, but angle of attack exhibits a huge scatter. The output roll angle is not a good estimation because it is prescribed as a fixed value, which is a general assumption made by BADA and others, which might be too simple.

The computation time for one profile on a standard desktop computer is about 1.5 s. This value, however, overestimates the computational cost of the presented algorithm. First, the code is experimental and offers wide potential for optimization. Second, once an error model is developed and the most relevant parameters are known, either the model could be simplified to yield only these or measurements of these parameters could be included in a future version of AMDAR reports.

Although the envisioned error model is not yet developed, the implications of the above results on the expected outcome may be estimated: From the Investigation of the Greenland Boundary Layer over Summit (IGLOS) field experiment (Drüe and Heinemann 2003), the pitch dependency of the true air temperature determined by a Dornier 228 standard temperature probe was estimated to amount roughly to 0.03 K $(°)^{-1}$. Hypothesizing that the same value applies for an Airbus A319 allows estimation of the error by neglecting a nonzero pitch (Fig. 9). The value is significantly nonzero at all levels (except one) and amounts about half of the typical systematic deviation of AMDAR temperature (Drüe et al. 2008). Such a correction would be capable of reducing systematic AMDAR errors while increasing the random error only rather slightly.

Although the scatter of some variables may by large, the flight dynamic state is estimated with good accuracy, on average. I hence conclude that the algorithm presented meets the objectives of the present study and may serve as basis for the envisioned error model or similar applications.

Acknowledgments. AMDAR data were supplied by Deutscher Wetterdienst within a continued cooperation on AMDAR data quality and application. The E-AMDAR technical coordinator, the WMO AMDAR technical coordinator, the Global Systems Division (GSD) of the Earth System Research Laboratory (ESRL) at the U.S. National Oceanic and Atmospheric Administration (NOAA) and the National Centers for Environmental Prediction (NCEP) of the U.S. National Weather Service (NWS) are thankfully acknowledged for supplying AMDAR unit metadata. Airbus A340 data were kindly supplied by the CARIBIC project through the Max-Planck-Institute for Chemistry, Atmospheric Chemistry Department, Mainz, Germany. Airbus A320 (ATRA) data were kindly supplied by DLR, Braunschweig, Germany.

REFERENCES

Ballish, B., and K. Kumar, 2006: Comparison of aircraft and radiosonde temperature biases at NCEP. Preprints, *10th Symp. on Integrated Observing and Assimilation Systems for the Atmosphere, Oceans, and Land Surface (IOAS-AOLS),* Boston, MA, Amer. Meteor. Soc., 3.5. [Available online at http://ams.confex.com/ams/pdfpapers/103076.pdf.]

——, and V. K. Kumar, 2008: Systematic differences in aircraft and radiosonde temperatures. *Bull. Amer. Meteor. Soc.,* **89,** 1689–1707.

Brenninkmeijer, C. A. M., and Coauthors, 2007: Civil aircraft for the regular investigation of the atmosphere based on an instrumented container: The new CARIBIC system. *Atmos. Chem. Phys.,* **7,** 4953–4976.

Cardinali, C., L. Isaksen, and E. Andersson, 2003: Use and impact of automated aircraft data in a global 4DVAR data assimilation system. *Mon. Wea. Rev.,* **131,** 1865–1877.

Cooper, W. A., and D. Baumgartner, 1989: Meeting review: Workshop on airborne instrumentation. NCAR Tech. Note NCAR/TN-330+PROC, 1–71.

Drüe, C., and G. Heinemann, 2001: Airborne investigation of arctic boundary-layer fronts over the marginal ice zone of the Davis Strait. *Bound.-Layer Meteor.,* **101,** 261–292.

——, and ——, 2003: Investigation of the Greenland atmospheric boundary layer over summit 2002 (IGLOS): Field phase report. Alfred Wegener Institute for Polar and Marine Research, Reports on Polar and Marine Research 447, 88 pp. [Available online at http://epic.awi.de/Publications/BerPolarforsch2003447.pdf.]

——, W. Frey, A. Hoff, and T. Hauf, 2008: Aircraft type-specific errors in AMDAR weather reports from commercial aircraft. *Quart. J. Roy. Meteor. Soc.,* **134,** 229–239.

——, T. Hauf, and A. Hoff, 2010: Comparison of boundary-layer profiles and layer detection by AMDAR and WRT/RASS at Frankfurt airport. *Bound.-Layer Meteor.,* **135,** 407–432.

Duke, G., 2009: *Air Traffic Control*. Midland, 112 pp.

EEC, 2009a: Base of Aircraft Data (BADA) aircraft performance modelling report. Eurocontrol Experimental Centre Technical/Scientific Rep. 2009-009, 68 pp. [Available online at http://www.eurocontrol.int/eec/gallery/content/public/document/eec/report/2009/009_BADA_Aircraft_performance_modelling.pdf.]

——, 2009b: User manual for the Base of Aircraft Data (BADA) revision 3.7. Eurocontrol Experimental Centre Technical/Scientific Rep. 2009-003, 102 pp. [Available online at http://www.eurocontrol.int/eec/gallery/content/public/document/eec/report/2009/003_BADA_3_7_User_manual.pdf.]

Erzberger, H., and L. Tobias, 1986: A time-based concept for terminal-area traffic management. National Aeronautics and Space Administration Ames Research Center Tech. Memo. 88243, 19 pp.

FAA, 1968: Maximum allowable airspeed indicator systems. Aircraft Certification Service, Federal Aviation Administration, Department of Transportation, Technical Standard Order Vol. TSO-C46a, 4 pp.

——, 1995: Temperature instruments. Aircraft Certification Service, Federal Aviation Administration, Department of Transportation, Technical Standard Order Vol. TSO-C43c, 4 pp.

Giraud, N., 2010: *Airfleets.net - The Book.* Airfleets.net, 168 pp.

Helms, D., K. L. Johnston, G. Sanger, B. Taubvurtzel, R. A. Petersen, A. Homans, and A. Hoff, 2009: Testing and deployment of the water vapor sensing system II. Preprints, *25th Conf. on International Interactive Information and Processing Systems (IIPS) for Meteorology, Oceanography, and Hydrology,* Phoenix, AZ, Amer. Meteor. Soc., 4A.5. [Available online at http://ams.confex.com/ams/89annual/techprogram/paper_149759.htm.]

Jenkinson, L. R., P. Simpkin, and D. Rhodes, 1999: *Civil Jet Aircraft Design*. Butterworth-Heinemann, 436 pp.

Moninger, W. R., R. D. Mamrosh, and P. M. Pauley, 2003: Automated meteorological reports from commercial aircraft. *Bull. Amer. Meteor. Soc.,* **84,** 203–216.

Morichon, L., 2006: Selected statistics in aircraft design. Diploma thesis, Department of Vehicle Technology and Aircraft Construction (Fahrzeugtechnik und Flugzeugbau), Hamburg University of Applied Sciences, 62 pp.

Nacass, P. L., 1992: Theoretical errors on airborne measurements of static pressure, impact temperature, air flow angle, and air flow speed. NCAR Tech. Note 385+STR, 62 pp.

Painting, J. D., 2003: AMDAR reference manual. World Meteorological Organization Tech. Rep. WMO-No. 958, 84 pp.

Pastre, C., 2000: What is new in our programmes? *EUMETNET News*, Vol. 6, EUMETNET, Paris, France, 13–15.

Press, W. H., S. A. Teukolsky, W. T. Vetterling, and B. P. Flannery, 1986: *Numerical Recipes in Fortran*. Cambridge University Press, 848 pp.

Renouard-Vallet, G., M. Saballus, G. Schmithals, J. Schirmer, J. Kallo, and K. A. Friedrich, 2010: Improving the environmental impact of civil aircraft by fuel cell technology: Concepts and technological progress. *Energy Environ. Sci.,* **3,** 1458–1468.

Schraff, C. and R. Hess, 2002: Datenassimilation für das LM (Data assimilation for the LM). *Promet,* **27** (3/4), 156–164.

Slattery, R., and Y. Zhao, 1997: Trajectory synthesis for air traffic automation. *J. Guidance Control Dyn.,* **20,** 232–238.

Stengel, R. F., 2004: *Flight Dynamics*. Princeton University Press, 845 pp.

Stickland, J., 2002: AMDAR status at December 2001. Expert Team on Observational Data Requirements and Redesign of the Global Observing System Fourth Session, World Meteorological Organization Report to Commission for Basic Systems Open Programme Area Group on Integrated Observing Systems, 9 pp.

Stickney, T. M., M. W. Shedlov, and D. I. Thompson, 1994: Goodrich total temperature sensors. Goodrich Corporation Tech. Rep. 5755, 32 pp.

Stoliker, F., and Coauthors, 2005: Introduction to flight test engineering. RTO AGARDograph 300 Flight Test Techniques Series RTO-AG-300 AC/323(SCI-FT3)TP/74, Vol. 14, Research and Technology Organisation of the North Atlantic Treaty Organization, 456 pp.

Taylor, A. D., 1997: Conformal map transformations for meteorological modelers. *Comput. Geosci.,* **23,** 63–75.

Tenenbaum, J., 1991: Jet stream winds: Comparisons of analyses with independent aircraft data over southwest Asia. *Wea. Forecasting,* **6,** 320–336.

Vörsmann, P., 1990: Meteopod, an airborne system for measurements of mean wind, turbulence, and other meteorological parameters. *Onde Electr.,* **70,** 31–38.

WMO AMDAR Panel, 2007: The international AMDAR program. World Meteorological Organization Information Flyer, 12 pp. [Available online at http://www.wmo.int/amdar/Publications/Final%20Production%20AMDAR%20Flyer.pdf.]